INTERNATIONAL JOURNAL FOR NUMERICAL METHODS IN FLUIDS
Int. J. Numer. Meth. Fluids 2008; **58**:687–708
Published online 26 February 2008 in Wiley InterScience (www.interscience.wiley.com). DOI: 10.1002/fld.1783

Solving the advection–dispersion equation with discontinuous Galerkin and multipoint flux approximation methods on unstructured meshes

Anis Younes*,† and Philippe Ackerer

Institut de Mécanique des Fluides et des Solides, Université Louis Pasteur/CNRS-UMR 7507, 2, rue Boussingault, 67000 Strasbourg, France

SUMMARY

In this work, we develop a new model to solve the advection–dispersion transport equation on unstructured triangular meshes. The model combines numerical methods that are specifically suited to achieve high accuracy for each type of equation without using the time splitting procedure. It is based on a combination of the upwind discontinuous Galerkin (DG) method for advection and the multipoint flux approximation (MPFA) method for dispersion.

In contrast to mixed finite elements, MPFA methods provide fluxes at element interfaces explicitly by weighted sums of discrete element concentrations. Therefore, the combination of DG and MPFA methods allows taking into account total flux boundary conditions while using different numerical techniques.

A theta-scheme time discretization is developed for advection and an implicit scheme for dispersion. Accuracy of the numerical model is shown by simulating (i) the transport of a tracer in a simplified bidimensional problem with highly unstructured mesh and (ii) a laboratory-scale experiment with high viscosity contrasts. Copyright © 2008 John Wiley & Sons, Ltd.

Received 13 June 2007; Revised 11 January 2008; Accepted 11 January 2008

KEY WORDS: discontinuous Galerkin methods; multipoint flux approximation methods; advection–dispersion equation; time splitting; unstructured meshes

1. INTRODUCTION

The most common mathematical model to simulate tracer transport in porous media is an advection–dispersion partial differential equation (PDE), which has the following formulation:

$$L(C) = \frac{\partial C}{\partial t} + \nabla \cdot (\mathbf{V}C) - \nabla \cdot (\mathbf{D} \cdot \nabla C) = 0 \qquad \mathbf{x} \in \Omega, \quad t \in [0, T] \tag{1}$$

*Correspondence to: Anis Younes, Institut de Mécanique des Fluides et des Solides, Université Louis Pasteur/CNRS-UMR 7507, 2, rue Boussingault, 67000 Strasbourg, France.
†E-mail: younes@imfs.u-strasbg.fr

Copyright © 2008 John Wiley & Sons, Ltd.

where $C(\mathbf{x},t)$ $[M/L^3]$ is the unknown concentration at location $\mathbf{x}$ and time t, and $\mathbf{D}$ $[L^2/T]$ is the dispersion tensor defined by

$$D_{ij}=(\alpha_{\mathrm{T}}|\mathbf{V}|+D_m)\delta_{ij}+(\alpha_{\mathrm{L}}-\alpha_{\mathrm{T}})\frac{v_i v_j}{|\mathbf{V}|},\quad i,j=1,2 \tag{2}$$

$L(C)$ is the differential operator; $\mathbf{V}$ $[L/T]$ is a given fluid velocity of components v_i; α_{L} and α_{T} $[L]$ are the longitudinal and transverse dispersivities; δ_{ij} is the Kronecker delta function; and D_m $[L^2/T]$ is the molecular diffusion coefficient. T is the end of the simulation time period starting at time zero.

Equation (1) is subject to the initial and boundary conditions:

$$\begin{aligned} C(\mathbf{x},0)&=C_0(\mathbf{x}), \quad \mathbf{x}\in\Omega\\ C(\mathbf{x},t)&=g_1(\mathbf{x},t) \quad (\mathbf{x}\in\partial\Omega^1, t>0)\\ (-\mathbf{D}\cdot\nabla C)\boldsymbol{\eta}_{\partial\Omega}&=g_2(\mathbf{x},t) \quad (\mathbf{x}\in\partial\Omega^2, t>0)\\ (\mathbf{V}C-\mathbf{D}\cdot\nabla C)\boldsymbol{\eta}_{\partial\Omega}&=g_3(\mathbf{x},t) \quad (\mathbf{x}\in\partial\Omega^3, t>0) \end{aligned} \tag{3}$$

where Ω is a bounded, polygonal open set of $\mathbb{R}^2$; $\partial\Omega^1$, $\partial\Omega^2$ and $\partial\Omega^3$ are partitions of the boundary $\partial\Omega$ of Ω corresponding to Dirichlet, Neumann and total flux boundary conditions; and $\boldsymbol{\eta}_{\partial\Omega}$ is the unit outward normal to the boundary $\partial\Omega$.

In many field situations, especially for small-scale simulations, the hyperbolic advective part of the PDE becomes dominant. In this case, standard numerical methods, such as finite elements or finite volumes, generate solution with numerical diffusion and/or non-physical oscillations.

On the other hand, the discontinuous Galerkin (DG) method has received more and more attention in the last two decades [1–3]. The flexibility of the DG method is its main advantage compared with other standard Euler schemes (finite volumes, finite elements), especially in handling complicated geometries, defining strategies for grid refinement or un-refinement and changing the degree of approximation from one element to the other. Moreover, the DG solution satisfies the mass conservation equation locally element by element.

Since the first DG method introduced in [4], the methods have been developed for hyperbolic problems [5–8] and elliptic problems [9–13]. A unified analysis for many DG methods for elliptic problems is given in [14].

When used for PDEs containing higher than first spatial derivatives, the DG methods have more degrees of freedom compared with the traditional finite element methods. This is often considered as a drawback of the DG or the local discontinuous Galerkin (LDG) method [15]. Moreover, the unknowns of the LDG method in any element depend, in general, on the neighbors of the element and the neighbors of the neighbors [1], which leads to less sparse matrix than with standard methods.

Contrary to the DG methods for elliptic problems, the DG methods for hyperbolic systems have been proven to be clearly superior to the already existing finite element methods [14]. With DG, we obtain a high-resolution scheme for advection that maintains the local conservation of finite volume methods but allows high-order approximations to enter through a variational formulation rather than by some hybridized difference or functional reconstruction [16].

Therefore, to solve the whole convection–diffusion equation, time splitting techniques are often applied to Equation (1). Advection and dispersion are then solved using different numerical techniques that are specifically suited to achieve high accuracy for each type of equations. In the

Copyright © 2008 John Wiley & Sons, Ltd.

DOI: 10.1002/fld

literature, several authors [3, 17–20] combined the DG method for advection with the mixed finite element method for dispersion.

The mixed finite element method is well suited for dispersion since it is locally conservative and can handle general irregular grids. However, it is well known [21, 22] that the discretization of the dispersion equation leads to an indefinite system matrix, which is generally circumvented by hybridization. In this case, the system is solved for the Lagrange multipliers and has more unknowns than the standard Eulerian methods (the number of edges instead of the number of elements).

Moreover, when the time splitting procedure is used, the total flux boundary conditions on $\partial\Omega^3$ cannot be prescribed. Indeed, in this case, we need the boundary flux for each operator while only the sum of the advective and the dispersive fluxes $g_3(\mathbf{x}, t)$ is given.

In this work, we describe a new scheme to solve the transport equation by using a combination of the DG method for advection and the multipoint flux approximation (MPFA) method for dispersion. The combination of DG and MPFA methods allows using different numerical techniques that are specifically suited to achieve high accuracy for each type of equations without using the time splitting procedure. Coupling different schemes to solve a PDE has already been applied to the transport equation and leads to an efficient solver. Siegel *et al.* [3] coupled DG with mixed hybrid finite element. Here, we chose the MPFA discretization, because this method requires only cell-centered concentrations as opposed to the mixed or the mixed hybrid finite element method.

The scheme is developed for unstructured triangular meshes. These meshes are suitable for practical problems with complex geometry and local mesh refinement. A theta-scheme time discretization is used for advection and a fully implicit scheme is used for dispersion.

For explicit advection schemes, limiters are necessary to remove unphysical oscillations from the numerical solution. In this work, a new slope limiter without any iterative procedure is developed for triangular elements.

For dispersion/diffusion, a symmetric formulation of the MPFA method is developed by changing the localization of the continuity points.

Numerical experiments, given in the last part of the paper, show the efficiency of the developed model for (i) a large range of grid Peclet numbers and highly unstructured meshes in the case of transport of tracer in a simplified bidimensional problem with uniform velocity and (ii) a laboratory-scale experiment performed with a high viscosity contrast between injected and displaced fluids.

2. DISCRETIZATION OF THE TRANSPORT EQUATION

The transport equation (1) is expressed in the following mixed form:

$$\begin{aligned} \frac{\partial C}{\partial t} + \nabla\cdot(\mathbf{V}C) + \nabla\cdot\mathbf{q}_\mathrm{D} &= 0 \\ \mathbf{q}_\mathrm{D} &= -\mathbf{D}\nabla C \end{aligned} \tag{4}$$

where $\mathbf{q}_\mathrm{D}$ is the dispersive flux, and $Q^D_{\partial Ei} = \int_{\partial Ei} \mathbf{q}_\mathrm{D}\cdot\boldsymbol{\eta}_{\partial Ei}$ is the total dispersive flux across the edge ∂Ei of E.

Over the element E, we assume a constant divergence of $\mathbf{q}_\mathrm{D}$, which is given by

$$\nabla\cdot\mathbf{q}_\mathrm{D} = \frac{1}{|E|}\sum_{\partial Ei} Q^D_{\partial Ei} \tag{5}$$

where $|E|$ is the area of E.

Copyright © 2008 John Wiley & Sons, Ltd.

DOI: 10.1002/fld

2.1. The upwind DG method for advection

The DG method is a high-resolution scheme for advection that achieves high-order accuracy while suppressing spurious oscillations. The method was used for multidimensional problems while incorporating practical slope limiters in [5].

With the DG method, the advective fluxes are uniquely defined by solving a Riemann problem at the interface of two elements. The DG's solution is shown to be total variation diminishing in [23].

In what follows, we recall briefly the mathematical developments of the upwind DG method. Additional information about the method can be found in [8, 24].

The physical domain Ω is discretized with triangular elements $\{E\}$. The DG method seeks weak solutions of (4) using the following discontinuous finite element space:

$$V_h = \{v \in L^\infty(\Omega) : v_h|_E \in V(E)\} \tag{6}$$

where $V(E)$ represents the approximation space on the triangular element E.

Basis functions can be discontinuous across inter-element boundaries. The approximate solution $C_h(\mathbf{x}, t)$ is expressed with linear basis functions ϕ_i^E on each element E as follows:

$$C_h(\mathbf{x}, t)|_E = \sum_{i=1}^{3} \tilde{C}_i^E(t)\phi_i^E(\mathbf{x}) \tag{7}$$

where $\tilde{C}_i^E(t)$ are the three unknown coefficients corresponding to the degrees of freedom.

The three unknowns for each element are the average value of the concentration defined at the triangle centroid $(\overline{x}_E, \overline{y}_E)$ and its deviations in each space direction [8] with the corresponding interpolation functions:

$$\begin{aligned}
\tilde{C}_1^E(t) &= \overline{C^E}, \quad \phi_1^E(x, y) = 1 \\
\tilde{C}_2^E(t) &= \frac{\partial C^E}{\partial x}, \quad \phi_2^E(x, y) = x - \overline{x}_E \\
\tilde{C}_3^E(t) &= \frac{\partial C^E}{\partial y}, \quad \phi_3^E(x, y) = y - \overline{y}_E
\end{aligned} \tag{8}$$

Contrary to the DG finite element method used in [3, 20] where unknowns correspond to the concentration at each node of the element, the used approximations do not depend on the geometry of the mesh elements but only on the space dimension ($\mathbb{R}^n$). For example, for quadrangular elements, the used scheme requires three unknowns to define the linear polynomial function instead of four (the number of nodes for quadrangles) as in [20].

The variational formulation of (4) over the element E using ϕ_i^E as test functions gives

$$\sum_j \frac{\mathrm{d}\tilde{C}_j^E}{\mathrm{d}t} \int_E \phi_j^E \phi_i^E - \sum_j \int_E \tilde{C}_j^E \phi_j^E \mathbf{V} \cdot \nabla \phi_i^E + \int_{\partial E} C^* \phi_i^E \mathbf{V} \cdot \boldsymbol{\eta}_{\partial E} + \int_E \frac{1}{|E|} \sum_{\partial Ej} Q_{\partial Ej}^D \phi_i^E = 0 \tag{9}$$

which can be expressed as

$$\sum_j \frac{\mathrm{d}\tilde{C}_j^E}{\mathrm{d}t} \int_E \phi_j^E \phi_i^E - \sum_j \int_E \tilde{C}_j^E \phi_j^E \mathbf{V} \cdot \nabla \phi_i^E + \int_{\partial E} C^* \phi_i^E \mathbf{V} \cdot \boldsymbol{\eta}_{\partial E} + \sum_{\partial Ej} Q_{\partial Ej}^D \int_E \phi_i^E = 0 \tag{10}$$

where C^* is the upstream concentration on ∂E.

Copyright © 2008 John Wiley & Sons, Ltd.

DOI: 10.1002/fld

The third term corresponds to the boundary integral over the three edges of the element E:

$$\int_{\partial E} C^* \phi_i^E \mathbf{V}\cdot\boldsymbol{\eta}_{\partial E} = \sum_{j=1}^{3} \frac{Q^E_{\partial Ej}}{|\partial Ej|} \int_{\partial Ej} C^*_{\partial Ej} \phi_i^E \tag{11}$$

where $\boldsymbol{\eta}_{\partial Ej}$ is the unit outward normal vector to the edge ∂Ej of length $|\partial Ej|$, and $Q^E_{\partial Ej}$ is the water flux across ∂Ej.

$C^*_{\partial Ej}$ is the concentration over ∂Ej, defined using an appropriate Riemann solver [25], which corresponds to the upstream concentration value:

$$C^*_{\partial Ej} = \lambda^E_{\partial Ej} \tilde{C}^E_{\partial Ej} + (1-\lambda^E_{\partial Ej}) \tilde{C}^{Ej}_{\partial Ej} \tag{12}$$

where Ej is the adjacent element of E such that ∂Ej is the common edge of E and Ej. At each edge, we define

$$\lambda^E_{\partial Ej} = \begin{cases} 1 & \text{if } \mathbf{V}\cdot\boldsymbol{\eta}_{\partial Ej} \geqslant 0 \\ 0 & \text{if } \mathbf{V}\cdot\boldsymbol{\eta}_{\partial Ej} < 0 \end{cases}$$

Substituting the three test functions ϕ_i^E into (9) leads to a system of three ordinary differential equations over E.

If we consider an element E with its three adjacent elements $E1$, $E2$ and $E3$ (Figure 1), the obtained system can be expressed in the following matrix form:

$$[A] \begin{pmatrix} \dfrac{\mathrm{d}\tilde{C}^E_1}{\mathrm{d}t} \\ \dfrac{\mathrm{d}\tilde{C}^E_2}{\mathrm{d}t} \\ \dfrac{\mathrm{d}\tilde{C}^E_3}{\mathrm{d}t} \end{pmatrix} = [B] \begin{bmatrix} \tilde{C}^E_1 \\ \tilde{C}^E_2 \\ \tilde{C}^E_3 \end{bmatrix} - [M^0] \begin{bmatrix} \tilde{C}^E_1 \\ \tilde{C}^E_2 \\ \tilde{C}^E_3 \end{bmatrix} - [M^1] \begin{bmatrix} \tilde{C}^{E1}_1 \\ \tilde{C}^{E1}_2 \\ \tilde{C}^{E1}_3 \end{bmatrix} - [M^2] \begin{bmatrix} \tilde{C}^{E2}_1 \\ \tilde{C}^{E2}_2 \\ \tilde{C}^{E2}_3 \end{bmatrix} - [M^3] \begin{bmatrix} \tilde{C}^{E3}_1 \\ \tilde{C}^{E3}_2 \\ \tilde{C}^{E3}_3 \end{bmatrix} - \begin{bmatrix} \sum_{\partial Ej} Q^D_{\partial Ej} \\ 0 \\ 0 \end{bmatrix} \tag{13}$$

with

$$A_{i,j} = \int_E \phi_j^E \phi_i^E, \quad B_{i,j} = \int_E \phi_j^E \mathbf{V}\cdot\nabla\phi_i^E$$

$$M^0_{i,j} = \lambda^E_{\partial E1} \frac{Q^E_{\partial E1}}{|\partial E1|} \int_{\partial E1} \phi_i^E \phi_j^E + \lambda^E_{\partial E2} \frac{Q^E_{\partial E2}}{|\partial E2|} \int_{\partial E2} \phi_i^E \phi_j^E + \lambda^E_{\partial E3} \frac{Q^E_{\partial E3}}{|\partial E3|} \int_{\partial E3} \phi_i^E \phi_j^E$$

$$M^1_{i,j} = (1-\lambda^E_{\partial E1}) \frac{Q^E_{\partial E1}}{|\partial E1|} \int_{\partial E1} \phi_i^E \phi_j^{E1}, \quad M^2_{i,j} = (1-\lambda^E_{\partial E2}) \frac{Q^E_{\partial E2}}{|\partial E2|} \int_{\partial E2} \phi_i^E \phi_j^{E2}$$

$$M^3_{i,j} = (1-\lambda^E_{\partial E3}) \frac{Q^E_{\partial E3}}{|\partial E3|} \int_{\partial E3} \phi_i^E \phi_j^{E3}$$

Copyright © 2008 John Wiley & Sons, Ltd.

DOI: 10.1002/fld

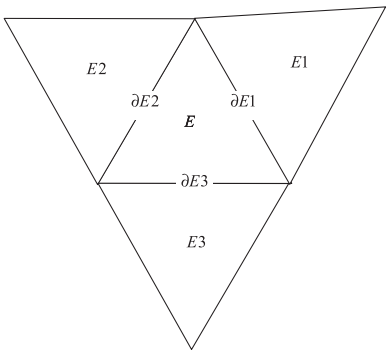

Figure 1. The triangular element E and its three neighbors.

All integrals are calculated analytically using (8). For example, the mass matrix reduces to

$$[A]=\begin{pmatrix} |E| & 0 & 0 \\ 0 & I_{xx} & I_{xy} \\ 0 & I_{xy} & I_{yy} \end{pmatrix} \tag{14}$$

with $I_{xx}=\int_E (x-\overline{x}_E)^2$, $I_{yy}=\int_E (y-\overline{y}_E)^2$ and $I_{xy}=\int_E (x-\overline{x}_E)(y-\overline{y}_E)$.

The matrix $[M^\ell]_{3\times 3}$ contains the contribution of the element $E\ell$ on E and vanishes if $\mathbf{V}\cdot\boldsymbol{\eta}_{\partial E\ell}\geqslant 0$.

We use the so-called theta-scheme for the temporal discretization of advection. For dispersion fluxes, we use a fully implicit time discretization.

Therefore, system (13) becomes

$$\begin{aligned} &\frac{1}{\Delta t}[A]\begin{pmatrix}\tilde{C}_1^E\\ \tilde{C}_2^E\\ \tilde{C}_3^E\end{pmatrix}^{n+1} -\theta[B]\begin{bmatrix}\tilde{C}_1^E\\ \tilde{C}_2^E\\ \tilde{C}_3^E\end{bmatrix}^{n+1} +\theta[M^0]\begin{bmatrix}\tilde{C}_1^E\\ \tilde{C}_2^E\\ \tilde{C}_3^E\end{bmatrix}^{n+1} +\theta[M^1]\begin{bmatrix}\tilde{C}_1^{E1}\\ \tilde{C}_2^{E1}\\ \tilde{C}_3^{E1}\end{bmatrix}^{n+1}\\ &+\theta[M^2]\begin{bmatrix}\tilde{C}_1^{E2}\\ \tilde{C}_2^{E2}\\ \tilde{C}_3^{E2}\end{bmatrix}^{n+1} +\theta[M^3]\begin{bmatrix}\tilde{C}_1^{E3}\\ \tilde{C}_2^{E3}\\ \tilde{C}_3^{E3}\end{bmatrix}^{n+1} +\begin{bmatrix}\sum_{\partial Ej} Q^D_{\partial Ej}\\ 0\\ 0\end{bmatrix}^{n+1}\\ &=\frac{1}{\Delta t}[A]\begin{pmatrix}\tilde{C}_1^E\\ \tilde{C}_2^E\\ \tilde{C}_3^E\end{pmatrix}^{n} +(1-\theta)[B]\begin{bmatrix}\tilde{C}_1^E\\ \tilde{C}_2^E\\ \tilde{C}_3^E\end{bmatrix}^{n} -(1-\theta)[M^0]\begin{bmatrix}\tilde{C}_1^E\\ \tilde{C}_2^E\\ \tilde{C}_3^E\end{bmatrix}^{n}\\ &-(1-\theta)[M^1]\begin{bmatrix}\tilde{C}_1^{E1}\\ \tilde{C}_2^{E1}\\ \tilde{C}_3^{E1}\end{bmatrix}^{n} -(1-\theta)[M^2]\begin{bmatrix}\tilde{C}_1^{E2}\\ \tilde{C}_2^{E2}\\ \tilde{C}_3^{E2}\end{bmatrix}^{n} -(1-\theta)[M^3]\begin{bmatrix}\tilde{C}_1^{E3}\\ \tilde{C}_2^{E3}\\ \tilde{C}_3^{E3}\end{bmatrix}^{n} \end{aligned} \tag{15}$$

Copyright © 2008 John Wiley & Sons, Ltd.

DOI: 10.1002/fld

Note that the full implicit scheme ($\theta=1$) does not require any flux or slope limiting procedure. However, these schemes are not suited for transient hyperbolic problems because they induce large numerical diffusion and accuracy demands time steps similar in size to that of explicit schemes.

In the developed model, the value of θ has to be fixed by the user before the simulation. The best value of θ can be problem dependent. When the explicit advection scheme ($\theta=0$) is used, the Courant–Friedrichs–Lewy (CFL) criterion has to be fulfilled for all elements in the domain. The concentrations obtained by the resolution of (15) may contain significant unphysical oscillations. In this case, limiters are necessary to remove these oscillations from the numerical solution before starting the new time step.

2.2. *The slope limiting*

It is known that when using constant cell approximations, the numerical diffusion due to upwinding is high enough to keep the scheme stable. However, by using higher-order approximation, the scheme produces non-physical oscillations near shocks. In such a case, the use of an appropriate slope limiter is crucial to ensure the stability of the method.

Many slope limiter techniques for unstructured triangular meshes are proposed in the literature. Chavent and Jaffré [26] introduced a limiter based on Van Leer's MUSCL limiter [27]. The degrees of freedom adopted are the concentrations at the vertices of each element. This technique may fail to smear completely the spurious oscillations and new extrema may be created at the midpoints of the grid edges [28]. To avoid this problem, a slope limiting operator that aims at eliminating oscillations at midpoint edges was proposed in [28]. Concentrations at vertices are then directly computed by using the reconstructed midpoint edge values. Other slope limiter techniques using the midpoints of edges as degrees of freedom have been developed for unstructured triangular elements (for example, [8, 29]).

Slope limiter techniques are often based on an iterative algorithm that may be central processing unit (CPU) consuming. In what follows, we briefly describe a new slope limiter for triangular elements with the family of linear basis and test functions adopted. The slope limiting does not contain any iterative procedure contrary to the scheme proposed in [28] for triangles. In order to satisfy the local maximum principle, the method ensures that no new extrema are created at the midpoints of the grid edges.

The concentration $\tilde{C}_{m_i}$ at (x_{m_i}, y_{m_i}), the midpoint of the edge ∂E_i (see Figure 1), is obtained from (7) and (8):

$$\tilde{C}_{m_i}=\overline{C^E}+\frac{\partial\tilde{C}^E}{\partial x}(x_{m_i}-\overline{x}_E)+\frac{\partial\tilde{C}^E}{\partial y}(y_{m_i}-\overline{y}_E) \tag{16}$$

The limiting is performed only on $\partial\tilde{C}^E/\partial x$ and $\partial\tilde{C}^E/\partial y$ in order to obtain reconstructed values $(\partial C^E/\partial x, \partial C^E/\partial y)$. $\overline{C^E}$ is kept unchanged to preserve the local mass balance.

The reconstructed midpoint values C_{m_i} have to verify the following two properties:

1. If $\tilde{C}_{m_i}$ is the concentration at the edge ∂Ei, the common edge of elements E and Ei, then C_{m_i} is between $\overline{C^E}$ and $\overline{C^{Ei}}$, respectively, the mean concentrations in E and Ei.
2. The reconstructed value C_{m_i} is as close as possible to the initial value $\tilde{C}_{m_i}$.

Copyright © 2008 John Wiley & Sons, Ltd.

DOI: 10.1002/fld

The above optimization problem is equivalent to the following one:

For a given $\widetilde{C_E}=(\tilde{C}_{m_1},\tilde{C}_{m_2},\tilde{C}_{m_3})$, find $\widehat{C_E}=(C_{m_1},C_{m_2},C_{m_3})$ solution to the problem:

$$\begin{aligned}
&\min\|\widehat{C_E}-\widetilde{C_E}\|_2 \quad \text{subject to linear constraints}\\
&\min(\overline{C^E},\overline{C^{E1}})\leqslant C_{m_1}\leqslant\max(\overline{C^E},\overline{C^{E1}})\\
&\min(\overline{C^E},\overline{C^{E2}})\leqslant C_{m_2}\leqslant\max(\overline{C^E},\overline{C^{E2}})\\
&\min(\overline{C^E},\overline{C^{E3}})\leqslant C_{m_3}\leqslant\max(\overline{C^E},\overline{C^{E3}})
\end{aligned}\tag{17}$$

This problem is solved without iterations in three steps:

- First, each $\widetilde{C}_{m_i}$ is set to its nearest value between $\overline{C^E}$ and $\overline{C^{Ei}}$:

$$C_{m_i}=\begin{cases}\min(\overline{C^E},\overline{C^{Ei}}) & \text{if } \widetilde{C}_{m_i}<\min(\overline{C^E},\overline{C^{Ei}})\\ \max(\overline{C^E},\overline{C^{Ei}}) & \text{if } \widetilde{C}_{m_i}>\max(\overline{C^E},\overline{C^{Ei}})\\ \widetilde{C}_{m_i} & \text{otherwise}\end{cases}\tag{18}$$

- Second, from each couple $(C_{m_i},C_{m_j})_{i\leqslant 3,j\leqslant 3,i\neq j}$, we calculate a couple $((\partial C^E/\partial x)_{ij},(\partial C^E/\partial y)_{ij})$ by solving the following system (obtained from (16)):

$$\begin{aligned}
(x_{m_i}-\overline{x}_E)\left(\frac{\partial C^E}{\partial x}\right)_{ij}+(y_{m_i}-\overline{y}_E)\left(\frac{\partial C^E}{\partial y}\right)_{ij}&=C_{m_i}-\overline{C^E}\\
(x_{m_j}-\overline{x}_E)\left(\frac{\partial C^E}{\partial x}\right)_{ij}+(y_{m_j}-\overline{y}_E)\left(\frac{\partial C^E}{\partial y}\right)_{ij}&=C_{m_j}-\overline{C^E}
\end{aligned}\tag{19}$$

- Finally, to ensure that no extrema are created at all midpoint edges, $(\partial C^E/\partial x,\partial C^E/\partial y)$ are obtained by

$$\begin{cases}\dfrac{\partial C^E}{\partial x}=\text{minmod}\left(\left(\dfrac{\partial C^E}{\partial x}\right)_{12},\left(\dfrac{\partial C^E}{\partial x}\right)_{13},\left(\dfrac{\partial C^E}{\partial x}\right)_{23}\right)\\ \dfrac{\partial C^E}{\partial y}=\text{minmod}\left(\left(\dfrac{\partial C^E}{\partial y}\right)_{12},\left(\dfrac{\partial C^E}{\partial y}\right)_{13},\left(\dfrac{\partial C^E}{\partial y}\right)_{23}\right)\end{cases}\tag{20}$$

where the minmod function is

$$\text{minmod}(a_1,\ldots,a_m)=\begin{cases}s\cdot\min\limits_{1\leqslant i\leqslant m}|a_i| & \text{if } s=\text{sign}(a_1)=\cdots=\text{sign}(a_m)\\ 0 & \text{otherwise}\end{cases}\tag{21}$$

2.3. The MPFA method for the dispersive fluxes

The MPFA method is an improved finite volume method. Contrary to the standard finite volume schemes, it allows one to treat rigorously the transport problem with a full discontinuous dispersion tensor on unstructured meshes.

Copyright © 2008 John Wiley & Sons, Ltd.

DOI: 10.1002/fld

The MPFA method has similar properties than the mixed finite element method. Indeed, both are locally conservative and handle general irregular grids on anisotropic heterogeneous domains. Several papers have been devoted to MPFA methods recently [30–33]. In contrast to mixed finite elements, MPFA methods provide fluxes at element interfaces explicitly by weighted sums of discrete element concentrations. The link between MPFA and mixed finite elements of Raviart Thomas or Brezzi–Douglas–Marini has been studied in [32, 34–37].

The basic idea of the MPFA method [30, 36] is to divide each triangle into three subcells (Figure 2). Inside the subcell $(\mathbf{x}_i, \mathbf{x}_i^2, \overline{\mathbf{x}}, \mathbf{x}_i^1)$ of the corner $\mathbf{x}_i$, we assume a linear variation of the concentrations between c_i^1, c_i^2 and $\overline{C^E}$, the concentration values at, respectively, midpoint edges $\mathbf{x}_i^1$ and $\mathbf{x}_i^2$ and the centre $\overline{\mathbf{x}}$ of the element E (Figure 2).

Therefore, subedge (half-edge) dispersive fluxes, taken positive for outflow, are given by

$$\begin{pmatrix} Q_i^1 \\ Q_i^2 \end{pmatrix} = \underbrace{\frac{1}{2|T_{\overline{\mathbf{x}}\mathbf{x}_i^1\mathbf{x}_i^2}|} \begin{pmatrix} (\mathbf{x}_i^1-\mathbf{x}_i)^\perp \mathbf{D}(\mathbf{x}_i^2-\overline{\mathbf{x}})^\perp & (\mathbf{x}_i^1-\mathbf{x}_i)^\perp \mathbf{D}(\overline{\mathbf{x}-\mathbf{x}_i^1})^\perp \\ (\mathbf{x}_i-\mathbf{x}_i^2)^\perp \mathbf{D}(\mathbf{x}_i^2-\overline{\mathbf{x}})^\perp & (\mathbf{x}_i-\mathbf{x}_i^2)^\perp \mathbf{D}(\overline{\mathbf{x}-\mathbf{x}_i^1})^\perp \end{pmatrix}}_{G_i^A} \begin{pmatrix} c_i^1-\overline{C^E} \\ c_i^2-\overline{C^E} \end{pmatrix} \tag{22}$$

where $|T_{\overline{\mathbf{x}}\mathbf{x}_i^1\mathbf{x}_i^2}|$ is equal to the area of the triangle spanned by the points $\overline{\mathbf{x}}$, $\mathbf{x}_i^1$ and $\mathbf{x}_i^2$, and the vector $(\mathbf{x}_i^1-\mathbf{x}_i)^\perp$ is obtained by a $\pi/2$ rotation of the vector $\mathbf{x}_i^1-\mathbf{x}_i$.

All subcells sharing the vertex i create an interaction volume (see Figure 3).

The discretization is accomplished by assuming continuous fluxes across each of the subedges of the interaction region and a weak continuity condition of the concentration across the same subedges. From these assumptions, an explicit discrete flux can be found after the resolution of a local linear system and elimination of the edge concentration for each subedge of the interaction volume. Each subedge dispersive flux can then be expressed explicitly as a weighted sum of the cell concentrations of elements forming the interaction volume. For example, for Figure 3 we obtain

$$Q_i^{D,1} = \sum_{k=1}^{5} t_i^k \overline{C^{E_k}} \tag{23}$$

where t_i^k are transmissibility coefficients.

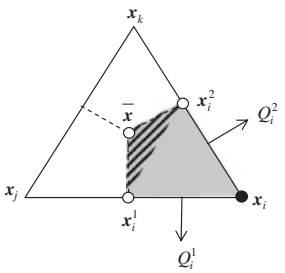

Figure 2. Triangle splitting into four subcells and linear concentration approximation on each subcell.

Copyright © 2008 John Wiley & Sons, Ltd.

DOI: 10.1002/fld

Note that contrary to the mixed or the mixed hybrid method, the computation of the fluxes requires cell-centred concentrations only with the MPFA method.

Equation (23) is expressed for the six half fluxes of element E. The sum of these fluxes gives the exchange of mass by dispersion between E and its adjacent elements. The sum of dispersive fluxes is then replaced in (15) to obtain the final discrete system to solve.

2.3.1. Localization of continuity points: symmetric or non-symmetric MPFA formulation. The MPFA method gives symmetric or non-symmetric dispersion matrix depending on the localization of the continuity points. Indeed, as shown in [31], symmetry of the global matrix is guarantied only if this property is respected for each local matrix G_i^A.

Continuity of the concentration is generally prescribed at the element-edge mid-point. This corresponds to $w=1$ (see Figure 4). In this case, the local matrix G_i^A in (22) is always non-symmetric.

However, as shown in [36], there is flexibility in the location of the continuity point. Its position can be chosen to lie at any point between the edge midpoint and the vertex (Figure 4).

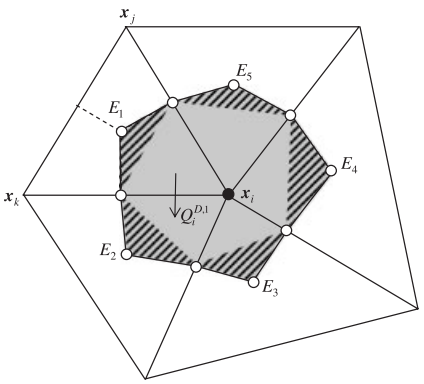

Figure 3. The interaction region sharing the vertex i.

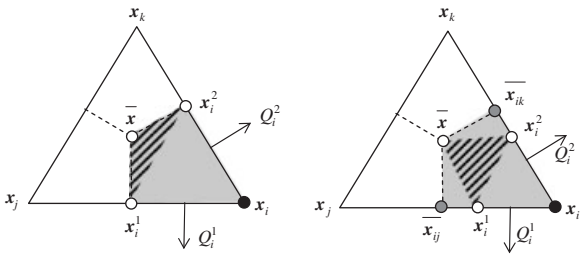

Figure 4. Two locations of the continuity point at the subcell interface. Local pressure support for $w=1.0$ and $\frac{2}{3}$.

Copyright © 2008 John Wiley & Sons, Ltd.

DOI: 10.1002/fld

The symmetry is achieved when the continuity point is localized at $w=\frac{2}{3}$ (Figure 4). In this case, $\mathbf{x}_i^1, \mathbf{x}_i, \mathbf{x}_i^2, \overline{\mathbf{x}}$ is a parallelogram and the local matrix G_i^A given in (22) becomes

$$Gs_i^A = \frac{1}{2|T_{\overline{\mathbf{x}}\mathbf{x}_i^1\mathbf{x}_i^2}|}\begin{pmatrix} (\overline{\mathbf{x}_{ij}}-\mathbf{x}_i)^\perp \mathbf{D}(\mathbf{x}_i^2-\overline{\mathbf{x}})^\perp & (\overline{\mathbf{x}_{ij}}-\mathbf{x}_i)^\perp \mathbf{D}(\overline{\mathbf{x}}-\mathbf{x}_i^1)^\perp \\ (\mathbf{x}_i-\overline{\mathbf{x}_{ik}})^\perp \mathbf{D}(\mathbf{x}_i^2-\overline{\mathbf{x}})^\perp & (\mathbf{x}_i-\overline{\mathbf{x}_{ik}})^\perp \mathbf{D}(\overline{\mathbf{x}}-\mathbf{x}_i^1)^\perp \end{pmatrix} \tag{24}$$

which is symmetric when replacing $\overline{\mathbf{x}}=(\mathbf{x}_i+\mathbf{x}_j+\mathbf{x}_k)/3$, $\overline{\mathbf{x}_{ij}}=(\mathbf{x}_i+\mathbf{x}_j)/2$, $\overline{\mathbf{x}_{ik}}=(\mathbf{x}_i+\mathbf{x}_k)/2$, $\mathbf{x}_i^1=\mathbf{x}_i/3+2\overline{\mathbf{x}_{ij}}/3$ and $\mathbf{x}_i^2=\mathbf{x}_i/3+2\overline{\mathbf{x}_{ik}}/3$.

Therefore, one can obtain a symmetric MPFA formulation for general triangular elements without any approximate numerical integration. Recall that for quadrilateral grids, the MPFA method leads to a symmetric matrix only in the case of parallelograms (constant Jacobian) [31].

Note that when the explicit advection scheme ($\theta=0$) is used in (15), the final system leads to a symmetric positive definite matrix. This allows using standard iterative solvers based on the conjugate gradient method, especially for very large systems that cannot be solved with direct solvers (because of memory requirement). The number of unknowns in this case is reduced to the total number of elements in the domain.

3. NUMERICAL EXPERIMENTS

Numerical experiments are performed to show the efficiency of the transport model based on DG and MPFA methods. In the first part, the advection–dispersion equation is solved for the simulation of a simplified bidimensional problem with highly unstructured mesh. Before simulating the transport equation, the flow equation is firstly solved with the mixed hybrid finite element method on triangles [38, 39] which gives accurate velocities with continuous normal component across the inter-element boundary.

In the second part, the developed model is used for the simulation of a very detailed laboratory experiment. Experiments at the laboratory scale are very useful for model verifications. Parameters, boundary conditions and state variables are known and the modeling of these experiments does not require any calibration. In this part, we simulate the experiments run by Loggia [40] who studied both stable and unstable flows occurring in a layered medium with density and viscosity contrasts.

3.1. Test case 1: transport of tracer on unstructured mesh with local mesh refinement

In this section, the developed DG_MPFA model is used for the resolution of the transport of tracer in a rectangular spatial domain Ω. The obtained results are compared with the analytical solution given in [41]. The physical domain is discretized with an unstructured mesh of 2070 nodes and 4004 elements as shown in Figure 5.

The mesh refinement is located close to transverse concentration fronts in order to increase the sensitivity of the spatial resolution. The flow is one-dimensional, horizontal and uniform ($v_x=1\,\mathrm{m/day}, v_y=0$), and the physical problem treated corresponds to a constant injection into a domain originally free of contaminant. The boundary conditions for the problem are of Dirichlet

Copyright © 2008 John Wiley & Sons, Ltd.

DOI: 10.1002/fld

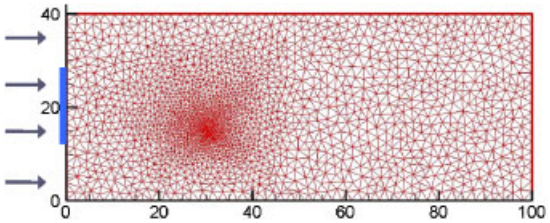

Figure 5. The physical domain Ω discretized with unstructured triangular elements.

type at the inflow with

$$C(0, y) = 0 \quad \forall y \in [0, 12[$$

$$C(0, y) = 1 \quad \forall y \in [12, 28]$$

$$C(0, y) = 0 \quad \forall y \in]28, 40]$$

A zero diffusive flux is prescribed at the outflow boundary. The results are given for different ranges of grid Peclet number using the following dispersion parameters:

- Sim1: $\alpha_l = 0.02m$, $\alpha_t = 0.005m$, $D_m = 0$, i.e. a grid Peclet number varying from 10.1 to 146.7. This corresponds to an advection-dominated problem.
- Sim2: $\alpha_l = 0.2m$, $\alpha_t = 0.05m$, $D_m = 0$, i.e. a grid Peclet number varying from 1.01 to 14.67.
- Sim3: $\alpha_l = 2m$, $\alpha_t = 0.5m$, $D_m = 0$, i.e. a grid Peclet number varying from 0.101 to 1.467.

For all the subsequent simulations, we consider the solution at time simulation $T = 60$ days. Simulations performed with $\theta = 0$, 0.6 and 1 are compared with the analytical solution.

With the explicit advective scheme ($\theta = 0$), the time step is restricted by the CFL condition. For triangular elements, the CFL is defined for each element E as follows [42]:

$$(\mathrm{CFL})_E = \frac{\sum_{j=1}^{3} |Q^E_{\partial Ej}|}{2|E|} \Delta t \tag{25}$$

with $Q^E_{\partial Ej}$ the water flux across the edge ∂Ej.

For the developed first-order scheme, the solution is stable only for CFL$\leqslant$0.5. Therefore, the global time step is limited by a critical value Δt_c:

$$\Delta t \leqslant \Delta t_c = \min_E \left(\frac{|E|}{\sum_{j=1}^{3} |Q^E_j|} \right) \tag{26}$$

The value of Δt_c can be very small for unstructured meshes and/or heterogeneous velocities. For the mesh of Figure 5, we obtain $\Delta t_c \simeq 0.12$ days.

In this work, the linear system of equations obtained by the transport is solved with a direct solver. Indeed, transport problems are often simulated for a steady-state flow (constant velocity during time). In this case, the transport matrix does not change and direct solvers are very appropriate since the system matrix has to be factorized only once. All simulations are performed with the combined unifrontal/multifrontal UMFPACK direct solver [43].

Copyright © 2008 John Wiley & Sons, Ltd.

DOI: 10.1002/fld

Results for sim1, sim2 and sim3 using different time steps are plotted in Figures 6–8. These figures also give the required CPU time and the relative L_1 error defined by

$$\mathrm{Err}_{L1} = \frac{\sum_{E=1}^{N_e} |E| |\overline{C}_E^{\mathrm{num}} - \overline{C}_E^{\mathrm{analy}}|}{\sum_{E=1}^{N_e} |E| |\overline{C}_E^{\mathrm{analy}}|} \tag{27}$$

where N_e is the total number of elements.

Results of Figures 6–8 show that

- The DG_MPFA model gives accurate results for the different advection/dispersion situations.
- The three schemes ($\theta = 0$, 0.6 and 1) give accurate results with small errors when small time steps are used ($\Delta t = \Delta t_c$).
- The schemes $\theta = 0.6$ and 1 are not limited by the CFL criteria. However, these schemes generate numerical diffusion for large time steps. The numerical diffusion is significant for the high advective case (sim1).
- The schemes $\theta = 0.6$ and 1 require similar CPU time. The scheme $\theta = 0.6$ gives results with much less numerical diffusion than the scheme $\theta = 1$. The error with $\theta = 0.6$ is generally 50% less significant than with $\theta = 1$.
- The scheme $\theta = 0.6$ with $\Delta t = 5\Delta t_c$ gives close results (with similar errors) than the explicit scheme with $\Delta t = \Delta t_c$ while the CPU time is reduced by a factor of 4.
- When used with $\Delta t = 25\Delta t_c$, the scheme $\theta = 0.6$ gives acceptable results. The CPU time is reduced by a factor of 10 compared with the explicit scheme.

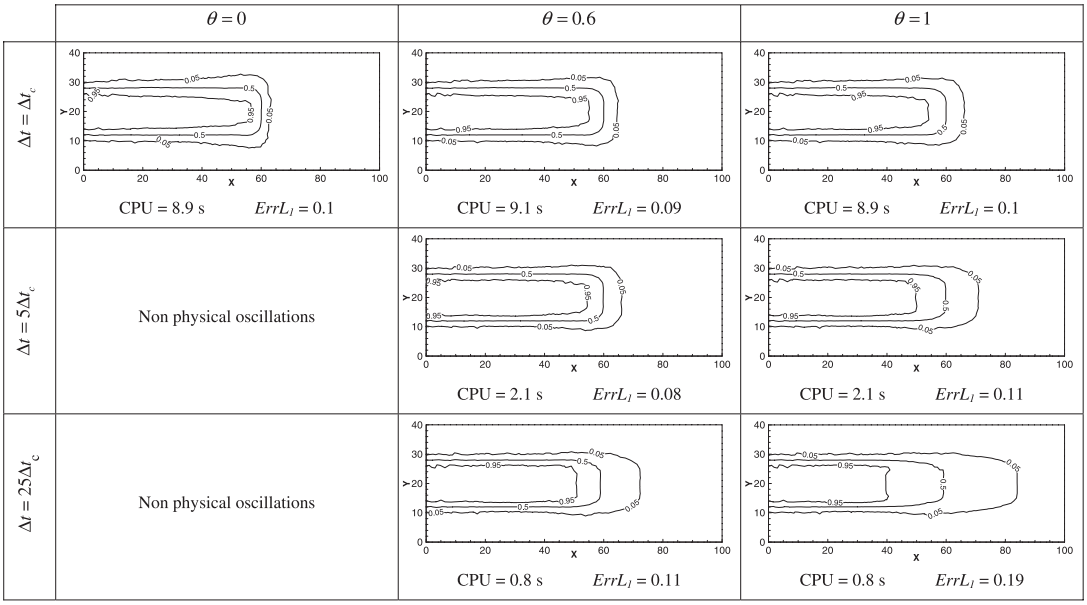

Figure 6. Concentration distribution, error and CPU time with DG_MPFA for different θ and $\alpha_l = 0.02m$, $\alpha_t = 0.005m$, $D_m = 0$.

Copyright © 2008 John Wiley & Sons, Ltd.

DOI: 10.1002/fld

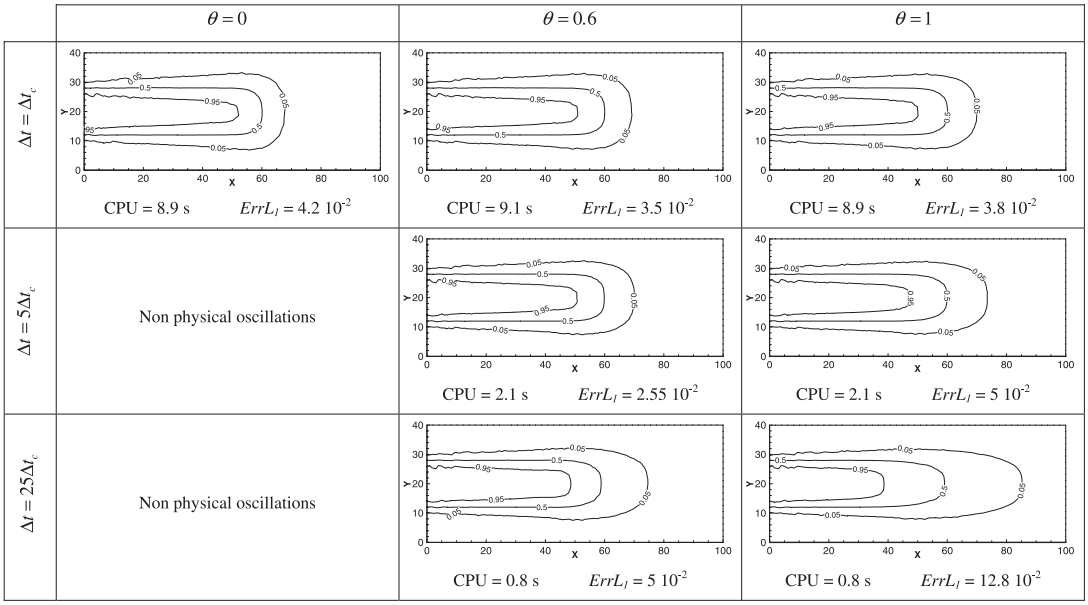

Figure 7. Concentration distribution, error and CPU time with DG_MPFA for different θ and $\alpha_l = 0.2m$, $\alpha_t = 0.05m$, $D_m = 0$.

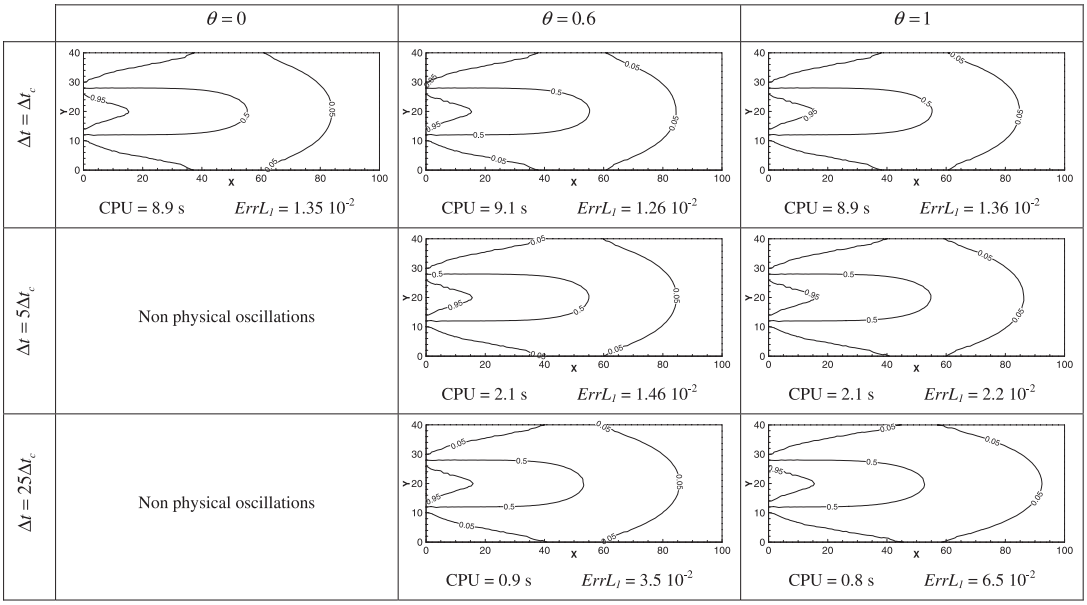

Figure 8. Concentration distribution, error and CPU time with DG_MPFA for different θ and $\alpha_l = 2m$, $\alpha_t = 0.5m$, $D_m = 0$.

Copyright © 2008 John Wiley & Sons, Ltd.

DOI: 10.1002/fld

A finite volume formulation of the model (called FV_MPFA) is easily obtained by removing the second and the third equations of system (15) for each element. In this case, the problem is solved for only one unknown (the mean concentration value) per element. The obtained scheme corresponds to the standard upwind finite volume scheme for advection.

The dominant advective case (sim1) is then simulated with FV_MPFA. Comparison between Figures 9 and 6 shows that contrary to the DG_MPFA model, the FV_MPFA model adds significant numerical diffusion to the solution for all values of θ.

In conclusion, the performed numerical experiments show that the DG_MPFA model gives accurate results. The scheme $\theta = 0.6$ is a good alternative to the full explicit scheme, especially for highly unstructured meshes. The error introduced by this scheme is limited, especially with moderate or high physical dispersion.

3.2. Test case 2: the Loggia's experiments

In this section, the developed DG_MPFA model is used for the simulation of the transport occurring in a layered medium with density and viscosity contrasts.

The experiments were run on a tank of $x = 4.5$ cm, $y = 4.5$ cm and $z = 30$ cm (Figure 10), filled with glass beads of various sizes distributed in layers. The characteristics of each layer are given in Table I. The longitudinal dispersivity is equal to the diameter of the beads and the transverse dispersivity is assumed to be 10 times smaller. The same porosity ($\varepsilon = 0.4$) is used for the four layers.

An input tank ensures homogeneous pressure and concentration at the upstream boundary of the layers. All experiments are performed at a fixed temperature of 30°C. A volumetric pump maintains a fixed flow rate at the entry of the domain. Measured concentrations are based on

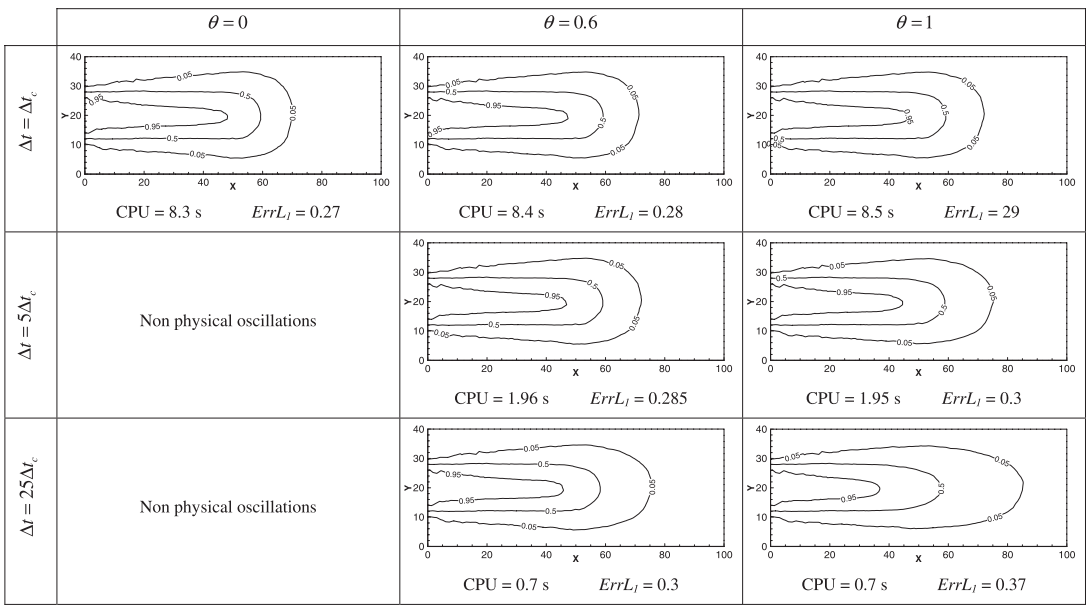

Figure 9. Concentration distribution, error and CPU time with FV_MPFA for different θ and $\alpha_l = 0.02m$, $\alpha_t = 0.005m$, $D_m = 0$.

Copyright © 2008 John Wiley & Sons, Ltd.

DOI: 10.1002/fld

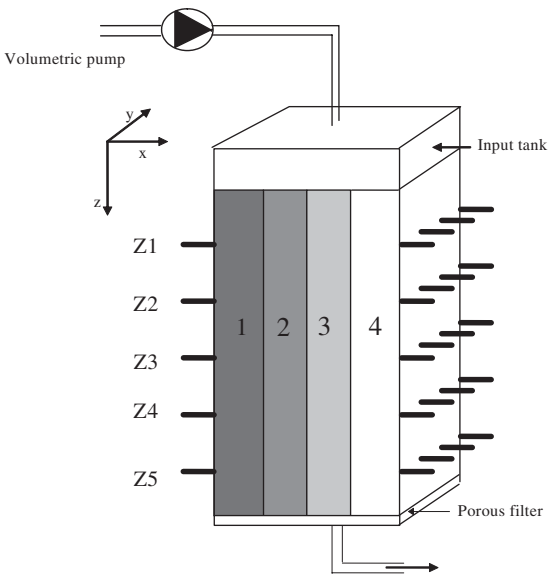

Figure 10. Experimental setup.

Table I. Porous media characteristics for the Loggia experiments.

Layer	H_i (m)	d_i (m)	k_i (m^2)
1	1.22×10^{-2}	85×10^{-6}	7.1×10^{-12}
2	1.08×10^{-2}	155×10^{-6}	23.7×10^{-12}
3	1.08×10^{-2}	194×10^{-6}	37.2×10^{-12}
4	1.22×10^{-2}	238×10^{-6}	55.8×10^{-12}

H, thickness; d, average diameter; k, permeability.

acoustic process. It allows obtaining the average of concentration at five fixed altitudes (Figure 10). A mixture of water–sucrose and water–glycerin is used to obtain large variations of viscosity between the injected and the displaced fluids.

For this problem, flow and transport are strongly coupled. At each time step, we have to solve the nonlinear system of PDEs describing the mass conservation of the fluid, the generalized Darcy's law and the transport equation of solute mass fraction:

$$\begin{aligned} \rho S\frac{\partial h}{\partial t}+\varepsilon\frac{\partial \rho}{\partial \omega}\frac{\partial \omega}{\partial t}+\rho\nabla\cdot\mathbf{q}&=0\\ \mathbf{q}&=-\mathbf{K}\left(\nabla h+\frac{\rho-\rho_0}{\rho_0}\nabla z\right)\\ \rho&=\rho_0+(\rho_1-\rho_0)\omega\\ \varepsilon\frac{\partial \omega}{\partial t}+\mathbf{q}\cdot\nabla\omega-\nabla\cdot\mathbf{D}\nabla\omega&=0 \end{aligned} \tag{28}$$

Copyright © 2008 John Wiley & Sons, Ltd.

DOI: 10.1002/fld

where P is the fluid pressure $[ML^{-1}T^{-2}]$, $\mathbf{q}$ Darcy's velocity $[LT^{-1}]$, ε the porosity [—], $\mathbf{K}=\mathbf{k}\rho_0 g/\mu$ the hydraulic conductivity tensor $[LT^{-1}]$, $\mathbf{k}$ the permeability tensor $[L^2]$, g the gravity acceleration $[LT^{-2}]$, ρ the fluid density $[ML^{-3}]$, μ the fluid dynamic viscosity $[ML^{-1}T^{-1}]$, ω the solute mass fraction [M of salt/M of fluid], $h=P/\rho_0 g+z$ the equivalent freshwater head, S the specific mass storativity related to head changes $[L^{-1}]$, ρ_1 the maximum fluid density and ρ_0 and μ_0 the density and viscosity of freshwater.

The flow system in (28) is solved using the lumped mixed finite element method [44]. The advection–dispersion transport equation of solute mass fraction is solved with the developed DG_MPFA model using $\theta=0.6$, which turns to be more efficient than $\theta=0$ even for this case where the flow matrix changes during computation (the values of the coefficients in the matrix are changed but not their location). For this problem, the small opening at the bottom of the tank induces very small time steps with the explicit advection scheme ($\theta=0$) due to the CFL constraint.

The time step management during the simulation is of heuristic type. The time step Δt^n is changed depending on the number of iterations k necessary to reach convergence in the following way:

$$\begin{aligned} &\text{if } k < 3, \quad \Delta t^n = 1.02\Delta t^{n-1} \\ &\text{if } 3 \leqslant k < 6, \quad \Delta t^n = 1.0\Delta t^{n-1} \\ &\text{if } 6 \leqslant k, \quad \Delta t^n = 0.9\Delta t^{n-1} \end{aligned} \tag{29}$$

System (28) is linearized with a Picard scheme and solved iteratively until the maximum variation on both h and C becomes small enough (less than 10^{-7} in this case). If the convergence is not reached after 20 iterations, the time step is divided by 2.

In order to test the developed model, two experiments were simulated, one with the injection of a tracer and the other with a fluid of high viscosity (Table II).

The following state equations were also established for the second experiment:

$$\begin{aligned} \mu &= \mu_0 \exp(2.02\omega/\omega_{\text{inj}}) \\ \rho &= \rho_0 + 53\omega/\omega_{\text{inj}} \end{aligned} \tag{30}$$

where ω_{inj} is the mass fraction of the injected solution.

The modeling of the experiments is based on the following concepts:

- Due to symmetry, the system is modeled in a two-dimensional cross section perpendicular to the layers (X–Z section).
- The input tank is not taken into consideration. It is assumed that the pressure is constant within that tank and that the solute mixing is instantaneous (compared with the travel time inside the porous medium) and perfect. Boundary conditions for flow and solute transport are prescribed pressure and mass fraction of the injected fluid.

Table II. Initial and injected fluid characteristics.

		Initial fluid		Injected fluid	
Exp.	q (cm/h)	Viscosity	Density	Viscosity	Density
1	9.89	0.0057	1124.0	0.0057	1117.0
2	4.95	0.0035	1132.0	0.0267	1185.0

Viscosity is in kg/m/s and density in g/l.

Copyright © 2008 John Wiley & Sons, Ltd.

DOI: 10.1002/fld

- The porous plate is taken into account and the measured flow rate is prescribed at the draining pipe. The measured permeability is $k = 5 \times 10^{-12}\,\mathrm{m}^2$ and porosity is equal to 0.2 for the porous plate. Longitudinal and transversal dispersivities are assumed to be equal to 85×10^{-6} and $8.5 \times 10^{-6}\,\mathrm{m}$. The last two parameters are not very sensitive, due to the small dimension of the porous plate. Dispersive fluxes are neglected at the outflow. The triangular discretization is obtained by subdivision of a 24×142 rectangular mesh.

The first experiment is a tracer test; the density and viscosity of the injected fluid and the displaced one are very close (Table II). The effect of the heterogeneities can be distinguished in the results (Figure 11). Experimental and simulated average concentrations are plotted in Figure 12.

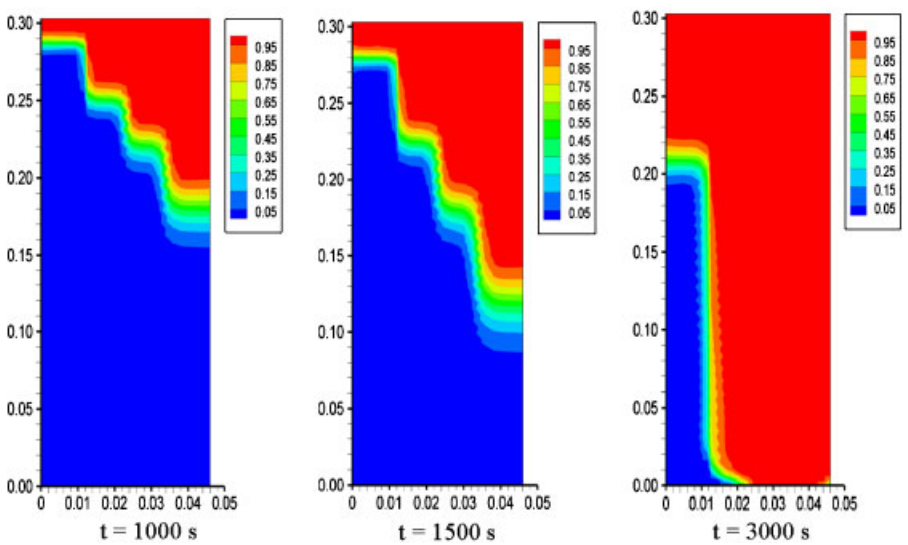

Figure 11. Mass fraction distribution (exp. 1).

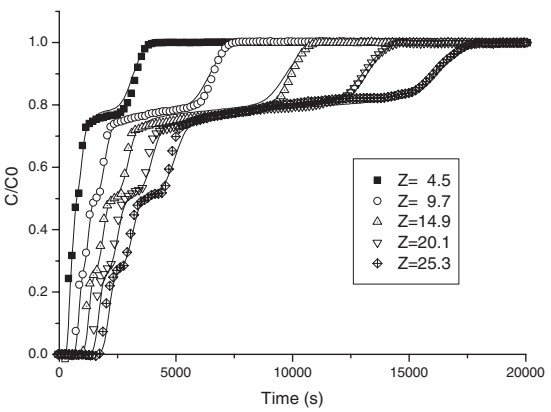

Figure 12. Measured (symbol) and computed breakthrough curves (exp. 1).

Copyright © 2008 John Wiley & Sons, Ltd.

DOI: 10.1002/fld

Although no model calibration has been performed, the match between measured and computed mass fractions is very good. The breakthrough of each layer is well reproduced by the model (time period with abrupt increase in mass fraction). The transition zones between the breakthroughs show a small increase in the concentration, due to mixing between the layers, which is also well reproduced by the simulation. [b]

The second experiment consists in the injection of a fluid with a viscosity, which is about 7.5 times higher than the viscosity of the displaced fluid. The match between simulated and measured mass fractions is still satisfactory (Figure 13). The effects of the heterogeneities are smoothed out by the viscosity contrast. The presence of the injected fluid having a higher viscosity reduces the effect of hydraulic conductivity. This phenomenon can be observed in Figures 14 and 15. Transverse

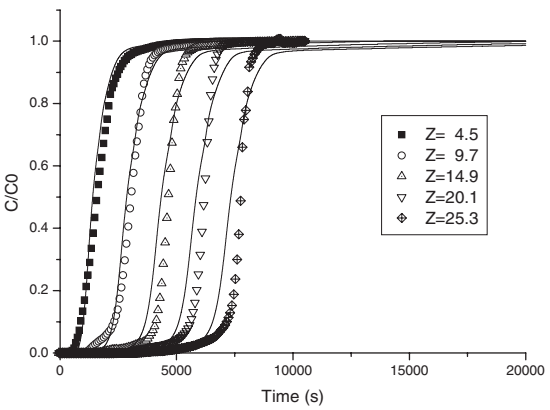

Figure 13. Measured (symbol) and computed breakthrough curves (exp. 2).

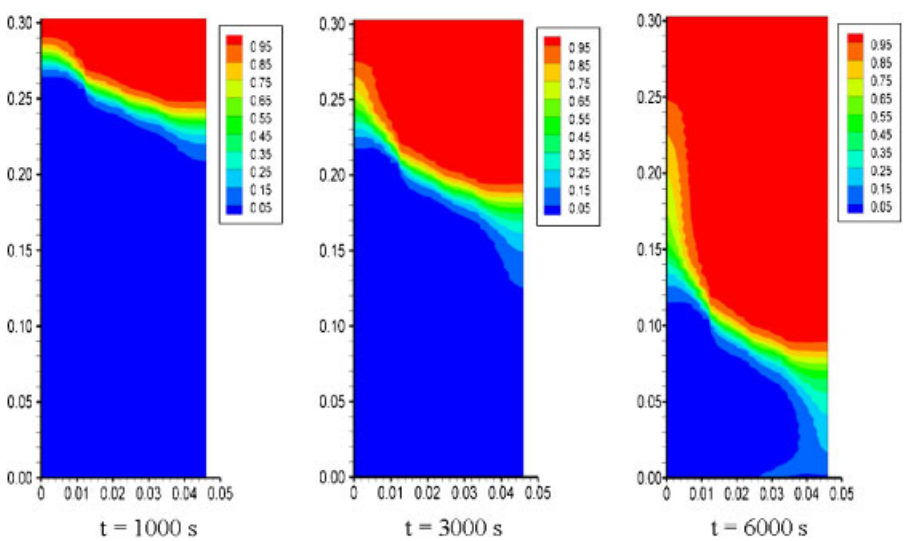

Figure 14. Mass fraction distribution (exp. 2).

Copyright © 2008 John Wiley & Sons, Ltd.

DOI: 10.1002/fld

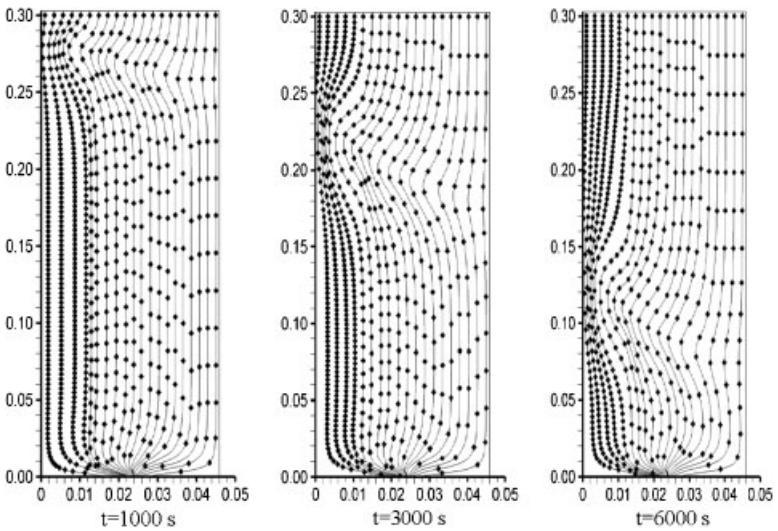

Figure 15. Pathlines and travel times (time lag between two markers: 400 s).

transfer (between layers) is increased by the viscosity contrast and the effect of heterogeneity is damped out.

4. CONCLUSION

With the time splitting procedure for the advection–dispersion equation, difficulties arise when the total flux boundary condition is prescribed. Indeed, in this case, we need the boundary flux for each operator while, only the sum of the advective and the dispersive fluxes is known.

To avoid this problem, a new model was developed to solve the advection–dispersion equation on unstructured triangular meshes. The model uses a combination of the upwind DG method for advection and the MPFA method for dispersion.

In contrast to mixed finite elements, MPFA methods provide fluxes at element interfaces explicitly by weighted sums of discrete element concentrations. The combination of DG and MPFA methods allows using different numerical techniques that are specifically suited to achieve high accuracy for each type of equations without using the time splitting procedure. A theta-scheme time discretization was developed for advection and an implicit scheme for dispersion. An efficient slope limiting technique that avoids iterative procedures was also developed for the explicit scheme.

The model was used for the simulation of the transport of a tracer on unstructured meshes with different advection/dispersion ratios and different θ. The DG_MPFA model gives accurate results and the scheme $\theta = 0.6$ can be a good alternative to the full explicit scheme, especially for highly unstructured meshes.

The model DG_MPFA was also tested for the simulation of a laboratory-scale experiment with high viscosity contrast. The obtained results are accurate and in agreement with the experimental results.

Copyright © 2008 John Wiley & Sons, Ltd.

DOI: 10.1002/fld

REFERENCES

1. Aizinger V, Dawson C, Cockburn B, Castillo P. The local discontinuous Galerkin method for contaminant transport. *Advances in Water Resources* 2001; **24**:73–87.
2. Cockburn B, Karniadakis GE, Shu CW (eds). *Discontinuous Galerkin Methods*: *Theory*, *Computation and Applications*. Lecture Notes in Computational Science and Engineering, vol. 11. Springer: Berlin, 2000.
3. Siegel P, Mosé R, Ackerer P, Jaffré J. Solution of the advection–diffusion equation using a combination of discontinuous and mixed finite elements. *International Journal for Numerical Methods in Fluids* 1997; **24**: 595–613.
4. Reed WH, Hill TR. Triangular mesh methods for the neutron transport equation. *Technical Report*, Los Alamos Scientific Laboratory, 1973.
5. Cockburn B, Shu C-W. The Runge–Kutta local projection P1-discontinuous Galerkin method for scalar conservation laws. *Mathematical Modelling and Numerical Analysis* 1991; **25**:337–361.
6. Cockburn B, Shu C-W. TVB Runge–Kutta local projection discontinuous Galerkin finite element method for conservation laws. II: General framework. *Mathematics of Computation* 1989; **52**(186):411–435.
7. Cockburn B, Hou S, Shu C-W. TVB Runge–Kutta local projection discontinuous Galerkin finite element method for conservation laws. III: One-dimensional systems. *Journal of Computational Physics* 1989; **84**:90.
8. Cockburn B, Shu C-W. The Runge–Kutta discontinuous Galerkin method for conservation laws. V: Multidimensional systems. *Journal of Computational Physics* 1998; **141**:199–224.
9. Wheeler MF. An elliptic collocation finite element method with interior penalties. *SIAM Journal on Numerical Analysis* 1978; **15**(1):152–161.
10. Oden JT, Babuska I, Baumann CE. A discontinuous hp finite element method for diffusion problems. *Journal of Computational Physics* 1998; **146**:491–519.
11. Cockburn B, Shu C-W. The local discontinuous Galerkin finite element method for convection–diffusion systems. *SIAM Journal on Numerical Analysis* 1998; **35**:2440–2463.
12. Rivière B, Wheeler MF, Girault V. Improved energy estimates for interior penalty, constrained and discontinuous Galerkin methods for elliptic problems I. *Computers and Geosciences* 1999; **3**:337–360.
13. Rivière B, Wheeler MF, Girault V. A priori error estimates for finite element methods based on discontinuous approximation spaces for elliptic problem. *SIAM Journal on Numerical Analysis* 2001; **39**(3):902–931.
14. Arnold DN, Brezzi F, Cockburn B, Marini LD. Unified analysis of discontinuous Galerkin methods for elliptic problems. *SIAM Journal on Numerical Analysis* 2002; **39**(5):1749–1779.
15. Li F, Shu C-W. A local-structure-preserving local discontinuous Galerkin method for the Laplace equation. *Methods and Applications of Analysis* 2006; **2**:215–234.
16. Kirby R. A posteriori error estimates and local time-stepping for flow and transport problems in porous media. *Ph.D. Thesis*, University of Texas at Austin, 2000.
17. Dawson CN. Godunov-mixed methods for advection flow problems equations in one space dimension. *SIAM Journal on Numerical Analysis* 1991; **28**:1282–1309.
18. Dawson C. Godunov-mixed methods for advection–diffusion equations in multidimensions. *SIAM Journal on Numerical Analysis* 1993; **30**:1315–1332.
19. Dawson C. Analysis of an upwind-mixed finite element method for nonlinear contaminant transport equations. *SIAM Journal on Numerical Analysis* 1998; **35**:1709–1724.
20. Ackerer Ph, Younes A, Mosé R. Modeling variable density flow and solute transport in porous medium: 1. Numerical model and verification. *Transport in Porous Media* 1999; **35**(3):345–373.
21. Brezzi F, Fortin M. *Mixed and Hybrid Finite Element Methods*. Springer: Berlin, 1991.
22. Chavent G, Roberts JE. A unified physical presentation of mixed, mixed hybrid finite elements and standard finite difference approximations for the determination of velocities in waterflow problems. *Advances in Water Resources* 1991; **14**:329–348.
23. Gowda V, Jaffré J. A discontinuous finite element method for scalar nonlinear conservation laws. *Rapport de recherche INRIA 1848*, 1993.
24. Cockburn B. Discontinuous Galerkin methods. *Zeitschrift fur Angewandte Mathematik und Mechanik* 2003; **11**:731–754.
25. Toro E. *Riemann Solvers and Numerical Methods for Fluid Dynamics*. Springer: Berlin, 1997.
26. Chavent G, Jaffré J. *Mathematical Models and Finite Elements for Reservoir Simulation*. North-Holland: Amsterdam, 1986.
27. Van Leer B. Towards the ultimate conservative scheme. V: A second order Godunov's method. *Journal of Computational Physics* 1979; **32**:101–136.

Copyright © 2008 John Wiley & Sons, Ltd.

DOI: 10.1002/fld

28. Hoteit H, Ackerer Ph, Mosé R, Erhel J, Philippe B. New two-dimensional slope limiters for discontinuous Galerkin methods on arbitrary meshes. *International Journal for Numerical Methods in Engineering* 2004; **61**:2566–2593.
29. Burbeau A, Sagaut P, Bruneau ChH. A problem-independent limiter for high-order Runge–Kutta discontinuous Galerkin methods. *Journal of Computational Physics* 2001; **169**:111–150.
30. Aavatsmark I. An introduction to multipoint flux approximations for quadrilateral grids. *Computational Geosciences* 2002; **6**:404–432.
31. Aavatsmark I, Barkve T, Bøe Ø, Mannseth T. Discretization on non-orthogonal, quadrilateral grids for inhomogeneous, anisotropic media. *Journal of Computational Physics* 1996; **127**:2–14.
32. Edwards MG, Rogers CF. Finite volume discretization with imposed flux continuity for the general tensor pressure equation. *Computers and Geosciences* 1998; **2**:259–290.
33. Klausen RA, Winther R. Convergence of multipoint flux approximations on quadrilateral grids. *Numerical Methods for Partial Differential Equations* 2006; **22**(6):1438–1454.
34. Eigestad GT, Klausen RA. On the convergence of the multi-point flux approximation O-method; numerical experiments for discontinuous permeability. *Numerical Methods for Partial Differential Equations* 2005; **21**: 1079–1098.
35. Klausen RA, Russell TF. Relationships among some locally conservative discretization methods which handle discontinuous coefficients. *Journal of Computational Geosciences* 2004; **8**(4):1–37.
36. Pal M, Edwards MG, Lamb AR. Convergence study of a family of flux-continuous, finite-volume schemes for the general tensor pressure equation. *International Journal for Numerical Methods in Fluids* 2006; **51**:1177–1203.
37. Vohralík M. Equivalence between lowest-order mixed finite element and multi-point finite volume methods on simplicial meshes. *Mathematical Modelling and Numerical Analysis* 2006; **40**(2):367–391.
38. Younes A, Ackerer Ph, Mosé R, Chavent G. A new formulation of the mixed finite element method for solving elliptic and parabolic PDE with triangular elements. *Journal of Computational Physics* 1999; **149**:148–167.
39. Chavent G, Younes A, Ackerer Ph. On the finite volume reformulation of the mixed finite element method for elliptic and parabolic PDE on triangles. *Computer Methods in Applied Mechanics and Engineering* 2003; **192**:655–682.
40. Loggia D. Etude par acoustique des écoulements de fluides miscibles en milieux poreux. Instabilités-hétérogèneités. *Thèse de Doctorat de l'Université Paris 7*, 1996.
41. Leij Feike J, Dane JH. Analytical solution of the one-dimensional advection equation and two- or three-dimensional dispersion equation. *Water Resources Research* 1990; **26**:1475–1482.
42. Putti M, Yeh W, Mulder W. A triangular finite volume approach with high-resolution upwind terms for the solution of groundwater transport equations. *Water Resources Research* 1990; **26**:2865–2880.
43. Davis TA, Duff IS. A combined unifrontal/multifrontal method for unsymmetric sparse matrices. *Technical Report TR-97-016*, Computer and Information Science and Engineering Department, University of Florida, 1997.
44. Younes A, Ackerer P, Lehmann F. A new mass lumping scheme for the mixed hybrid finite element method. *International Journal for Numerical Methods in Engineering* 2006; **67**(1):89–107.

Copyright © 2008 John Wiley & Sons, Ltd.

DOI: 10.1002/fld